Theoretical Investigation of the Second-Order Harmonic Distortion in the AM Response of 1.55 μm F–P and DFB Lasers

Geert Morthier, Frank Libbrecht, Klaus David, Patrick Vankwikelberge, and Roel G. Baets, *Member, IEEE*

Abstract—**Numerical calculations of the second-order harmonic distortion in the amplitude modulation-response of Fabry–Perot and distributed feedback lasers are presented and the influence of several nonlinearities, such as longitudinal spatial hole burning, gain suppression, and relaxation oscillations is considered in detail. Our analysis is valid for modulation frequencies ranging from a few megahertz to well beyond the resonance frequency of the relaxation oscillation. The numerical calculation of the distortion is based on the laser model CLADISS [1] and consists of an extended small signal solution (up to second-order) of the set of coupled wave equations and the local carrier density rate equations.**

The distortion is investigated for Fabry–Perot lasers for which the effects of spontaneous emission and gain suppression can be clearly illustrated and for DFB lasers where the emphasis is on the influence of spatial hole burning and its combination with other nonlinearities. Various effects are discussed, e.g., the occurrence of a dip in the frequency dependence of the distortion resulting from the combination of spatial hole burning and relaxation oscillation contributions in some cases and the occurrence of a dip in the bias dependence when spatial hole burning and gain suppression contributions cancel each other.

I. Introduction

HARMONIC and intermodulation distortion in the AM response of laser diodes can have a detrimental influence on the performance of analog optical communication systems, for which DFB lasers are generally regarded as most desirable light sources [3], [4]. Such lasers can operate in a stable, single longitudinal mode, which results in a reduced intensity noise and a reduced chromatic fiber dispersion. One source of distortion, typical for DFB lasers, is longitudinal spatial hole burning, i.e., the mode loss and gain are power dependent due to a longitudinal variation in the carrier density, caused by a longitudinal variation in the optical power density. Other nonlinearities, which are present in all semiconductor lasers, have their origin in gain suppression, spontaneous emission, and in the relaxation oscillations.

Manuscript received September 10, 1990; revised March 21, 1991. This work was supported by the European RACE Project R-1010 (CMC). The work of G. Morthier and F. Libbrecht was supported by the Belgian Institute for the Scientific Research in Industry and Agriculture (IWONL) and the work of P. Vankwikelberge was supported by the Belgian National Fund for Scientific Research (NFWO).

The authors are with the Laboratory of Electromagnetism and Acoustics, University of Gent—IMEC, B-9000 Gent, Belgium.

IEEE Log Number 9101365.

Numerical simulations of the distortion, which allow to assess the impact of several nonlinearities and the importance of different laser parameters in this, can eventually lead to a substantial reduction of the distortion and are therefore of prime interest. So far, the influence of only a few nonlinearities on the distortion has been studied. Subkjaer *et al.* [5] and Lau *et al.* [6] have reported the effect of relaxation oscillations and spontaneous emission on the distortion in Fabry–Perot lasers. Maeda *et al.* [7] also included carrier diffusion in their analysis which, however, was still restricted to F–P lasers and did not include gain suppression. Gain suppression was first taken into account by Darcie *et al.* [8], who studied the damping of the relaxation oscillation in F–P as well as DFB lasers. Recently, it has been shown by Takemoto *et al.* [9] that the static distortion in DFB lasers, which is mainly due to longitudinal spatial hole burning and can be calculated from the static L–I relation, is minimum for κL values around 1. Lin *et al.* [10], [11] found a dip in the bias dependence of the distortion in DFB lasers, which they explained as a result of leakage currents.

In the present analysis, we report calculations of the distortion over the full range from low to high (in the vicinity of the relaxation oscillation resonance frequency) modulation frequencies. A multimode longitudinal laser model, called CLADISS [1], [2], that solves the coupled wave equations and the carrier density rate equations has been used for this. This model can take into account gain suppression, spatial hole burning, spontaneous emission, side modes, and dynamic effects in a detailed way. Thermal effects on the other hand are not taken into account, which implies that only modulation frequencies above ± 1 MHz will be considered. We neither take into account leakage currents and refer to [11] for this. Our analysis confirms that the spatial hole burning induced static distortion in DFB lasers is minimum for κL values around 1. It is furthermore found that the dip in the bias dependence of the distortion can also be explained as resulting from a compensation of the spatial hole burning induced distortion by the gain suppression. In addition, a dip in the frequency dependence, resulting from the compensation of the spatial hole burning induced distortion by the relaxation oscillation, is sometimes found.

This paper is organized as follows. In the first section,

0018-9197/91/0800-1990$01.00 © 1991 IEEE

the numerical model for the accurate calculation of the distortion is shortly described. This model is first applied to a simple Fabry–Perot laser in the second section. Since spatial hole burning has almost no influence in these lasers, the influence of gain suppression, spontaneous emission, and relaxation oscillations can be clearly illustrated for such lasers. Next, a few examples of DFB lasers are considered to illustrate and discuss the effect of spatial hole burning and its combination with other nonlinearities. In most cases, our numerical results are compared with analytical expressions obtained from simple rate equations. In this way, the influence of certain parameters becomes clear, while at the same time some restrictions of the rate equations (i.e., discrepancies from the results obtained with the longitudinal model) can be found. Such a rate equation description is furthermore only possible for a limited number of DFB laser structures. Finally, a few conclusions on how to reduce the distortion are given.

II. The Longitudinal Model

Our model solves the set of time dependent, coupled traveling wave equations, which determine the optical field inside the laser cavity and which can be derived from Maxwell's equations in the slowly varying amplitude approximation [12] and the approximations related to the coupled mode theory [13]. The model is limited to index-guided lasers and assumes that only the lowest order TE mode is present. The forward (+) and backward (−) propagating parts of the lateral electrical laser field, consisting of several longitudinal modes, can then be written as

$$E_{y,q}^{\pm}(x, y, z, t) = \phi(x, y)\,\mathrm{Re}\left\{\sum_q E_q^{\pm}(z, t)\exp\left(j\omega_q t \mp j\beta_{rq} z\right)\right\}. \quad (1)$$

The transverse–lateral field distribution $\phi(x, y)$ is assumed to be independent of time and axial position and to be the same for each longitudinal mode q. β_{rq} is a reference propagation constant, which is chosen as the Bragg wavenumber $m\pi/\Lambda$ when a grating of order m is present. In the absence of a grating, β_{rq} is chosen as the propagation constant at the reference frequency ω_q of the lowest order TE mode of the unperturbed waveguide (i.e., the waveguide without carrier injection). The complex amplitudes $E_q^{\pm}$ are slowly varying in time with respect to ω_q (a reference frequency to be chosen close to the expected emission frequency) and can be transformed as [1]

$$E_q^{\pm}(z, t) = r_q^{\pm}(z, t)\exp\left[j\phi_q^{\pm}(z, t) + j\int^t \Delta\omega_q(\tau)\,d\tau\right] \quad \text{with } \phi_q^{-}(z = 0, t) = 0. \quad (2a)$$

Both $r_q^{\pm}$ and $\phi_q^{\pm}$ are real functions of z and t. The last boundary condition of (2a) implies that the instantaneous frequency of the laser $\bar{\omega}_q$ (which hardly varies along the laser cavity if the dynamic excitation is slow with respect to the round-trip time) is defined as the instantaneous frequency of the backward field at the left facet ($z = 0$). The instantaneous frequency of the laser then becomes

$$\bar{\omega}_q(t) = \omega_q + \frac{d}{dt}\arg\left[E_q^{-}(z = 0, t)\right] = \omega_q + \Delta\omega_q(t). \quad (2b)$$

The coupled wave equations, e.g., for the forward propagating wave, can now be written as [1]

$$\frac{\partial r_q^{+}}{\partial z} + \frac{1}{v_g}\frac{\partial r_q^{+}}{\partial t} - \left(\Delta\beta_{iq} + \frac{J_{\mathrm{sp}}}{(r_q^{+})^2}\right) r_q^{+} = |\kappa^{+}|\cos\left(\phi_\kappa^{+} + \phi_q^{-} - \phi_q^{+}\right) r_q^{-}$$

$$\frac{\partial\phi_q^{+}}{\partial z} + \frac{1}{v_g}\frac{\partial\phi_q^{+}}{\partial t} + \frac{1}{v_g}\Delta\omega_q + \Delta\beta_{rq} = \frac{r_q^{-}}{r_q^{+}}|\kappa^{+}|\sin\left(\phi_\kappa^{+} + \phi_q^{-} - \phi_q^{+}\right). \quad (3)$$

Similar equations hold for r_q^{-} and ϕ_q^{-}. $|\kappa^{+}|$ and ϕ_κ^{+} are amplitude and phase of κ^{+}, the coupling coefficient from backward to forward propagating wave. $\Delta\beta_{rq}$ and $\Delta\beta_{iq}$ are the real and imaginary part of the Bragg deviation, i.e., the difference between the propagation constant of the excited waveguide and the reference propagation constant:

$$\Delta\beta_{rq} = \beta_q - \beta_{rq} + \frac{\bar{\omega}_q}{c}\Delta n_{r,q}$$

$$\Delta\beta_{iq} = 0.5(\Gamma g_q - \alpha_{\mathrm{int}}). \quad (4)$$

α_{int} represents the internal losses and g_q the power gain in the active region for mode q. The gain function, which includes gain suppression, is of the form

$$g_q = A(\bar{\omega}_q)\left(N - N_{tq}(\bar{\omega}_q)\right)\cdot\left\{1 - \sum_p \epsilon_{\mathrm{sp}}(\bar{\omega}_q, \bar{\omega}_p)\left((r_p^{+})^2 + (r_p^{-})^2\right)\right\} \quad (5a)$$

with A being the differential gain. Δn_r expresses the change in the real part of the refractive index, induced by the carrier density N:

$$\Delta n_r = -\frac{2\bar{\omega}_q}{c}\alpha_{lw}(\bar{\omega}_q)\,A(\bar{\omega}_q)\,N(z, t). \quad (5b)$$

α_{lw} is the linewidth enhancement factor. The functions g_q and $\Delta n_{r,q}$ are found by curve fitting on the results obtained with the models of [14]. The $J_{\mathrm{sp}}/(r_q^{+})^2$ term in (3) represents the spontaneous emission that couples into the mode [1]. For power normalized field intensities, J_{sp} can be written as [1]

$$J_{\mathrm{sp}} = \tfrac{1}{4}wd\beta_{\mathrm{sp}}h\bar{\omega}_q BN^2 \quad (5c)$$

with β_{sp} being the spontaneous emission factor [15].

The carrier density varies with position and is determined by the equation

$$\frac{\partial N}{\partial t} = \frac{\eta J}{qd} - \frac{N}{\tau} - BN^2 - CN^3 - \sum_q \frac{\Gamma g_q}{h\bar{\omega}_q wd} \{(r_q^+)^2 + (r_q^+)^2\}. \quad (6)$$

The calculation of the distortion now proceeds in three steps. First, a static solution for some bias current is found through a Newton–Raphson iteration on the nonlinear equations (3)–(6), in which the time derivative terms have been dropped. In order to take into account longitudinal spatial hole burning, the cavity is divided in small sections, in which a uniform carrier density can be assumed, and the propagation is calculated by multiplication of the propagator matrices for each small section.

A small sinusoidal modulation current J_1 with a modulation frequency $\Omega/2\pi$ is then superimposed on the bias current. All variables are now expanded as

$$\begin{aligned} r_q^{\pm}(z, t) &= r_{qo}^{\pm}(z) + \text{Re}\{r_{q1}^{\pm}(z, \Omega)\, e^{j\Omega t} + r_{q2}^{\pm}(z, \Omega)\, e^{2j\Omega t}\} \\ \phi_q^{\pm}(z, t) &= \phi_{qo}^{\pm}(z) + \text{Re}\{\phi_{q1}^{\pm}(z, \Omega)\, e^{j\Omega t} + \phi_{q2}^{\pm}(z, \Omega)\, e^{2j\Omega t}\} \\ N(z, t) &= N_o(z) + \text{Re}\{N_1(z, \Omega)\, e^{j\Omega t} + N_2(z, \Omega)\, e^{2j\Omega t}\} \\ \Delta\bar{\omega}_q(t) &= \Delta\bar{\omega}_{qo} + \text{Re}\{\Delta\bar{\omega}_{q1}(\Omega)\, e^{j\Omega t} + \Delta\bar{\omega}_{q2}(\Omega)\, e^{2j\Omega t}\} \\ J(t) &= J_o + \text{Re}\{J_1 e^{j\Omega t}\} \end{aligned} \quad (7)$$

where the terms with subscript o refer to the static solution, the terms with subscript 1 to the linear small signal modulation and the terms with subscript 2 to the second-order harmonic distortion.

In a second step, (3)–(6) are linearized by substituting only the static and the first-order terms (with subscript 1) of (7) into (3)–(6). The derivatives with respect to z are then replaced by finite differences (over the same sections as in the static analysis), which results in a set of linear algebraic equations. These equations are too extended to write down here, but they can be solved by standard numerical techniques. This step allows to determine the small-signal AM and FM responses.

In the third step, the second-order harmonic distortion is finally calculated by substituting the full expansions of (7) in (3)–(6), and by considering only the terms with pulsation 2 Ω in the resulting expressions. Since the terms with subscripts o and 1 are now known quantities, this results in a linear system in the second-order quantities (with subscript 2). The excitation is thus no longer an ac current, but consists of products of the first-order quantities. It must be noticed that with this method, the distortion in the FM and the AM responses are calculated simultaneously. In this paper, however, we will concentrate on the distortion in the AM response. In principle, this method can also be extended for a calculation of the third-order harmonic distortion.

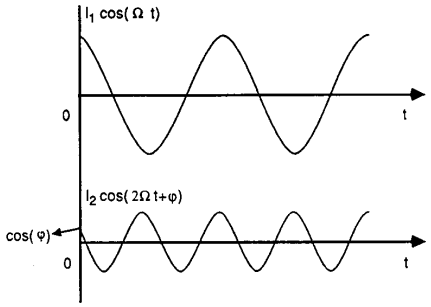

Fig. 1. Time variation of the first (I_1) and second-order (I_2) intensity and definition of the phase of the second-order harmonic distortion.

It should be remarked that the first- and second-order quantities are complex and thus characterized by a phase. Since both quantities vary with a different frequency, the definition of the phase needs some clarification. To this end, Fig. 1 shows the time variation of both the first- and second-order output power, the latter one having a phase φ. In the following, just as in Fig. 1, the time origin is always chosen so that the first-order intensity varies as cos (Ωt). The phase of the second-order harmonic distortion can be more exactly defined as the phase difference between the second order output power and the square of the first order output power. At static modulation frequencies, the phase of the distortion can also be derived from the L–I relation. In this case, a phase 0 (π) results when the efficiency in(de-)creases with bias level. However, as will become clear further, it is mainly the phase difference between different contributions to the distortion that is important.

III. Distortion in Fabry–Perot Lasers: Numerical Results and Discussion

The second-harmonic distortion in single longitudinal mode Fabry–Perot lasers, as calculated with our model, has its origin mainly in the gain suppression (which results in a power dependence of the gain), spontaneous emission (only at small bias currents), and relaxation oscillations (at high modulation frequencies). The relative importance of each of the effects can easily be estimated from a small signal solution (up to second-order) of the single mode rate equations.

$$\frac{dI}{dt} = (G - \Gamma) I + R \quad (8a)$$

$$\frac{dN}{dt} = \frac{J}{q} - s(\mathfrak{N}) - GI \quad (8b)$$

in which I represents the number of photons and N the number of electrons in the cavity. R is the spontaneous emission rate (corresponding with the J_{sp} term of the longitudinal model), G is the modal gain, and Γ is the loss. J is the injected current and S represents the spontaneous

carrier recombination (via traps, bimolecular and Auger recombination):

$$S(N) = \frac{N}{\tau} + BN^2 + CN^3. \tag{9}$$

The gain can be approximated as

$$G = (AN - B)(1 - \epsilon I) = G_0(N)(1 - \epsilon I) \tag{10}$$

where the I dependence is caused by gain suppression.

The second-order harmonic distortion can be determined after use of the expansions:

$$J = J_0 + J_1 e^{j\Omega t} \tag{11a}$$

$$I = I_0 + I_1 e^{j\Omega t} + I_2 e^{2j\Omega t} \tag{11b}$$

$$N = N_0 + N_1 e^{j\Omega t} + Ne^{2j\Omega t} \tag{11c}$$

$$S = S(N_0) + S_N(N - N_0) + \tfrac{1}{2}S_{NN}(N - N_0)^2 \tag{11d}$$

in which J_0 represents the bias current and J_1 the sinusoidal modulation current. Substitution of these expressions in the rate equations (8) yields, after some manipulations, for the AM response and the second-harmonic distortion of a Fabry–Perot laser:

$$\frac{I_1}{I_0} = \frac{A(J_1/q)}{\{(j\Omega + S_N + AI_0)(j\Omega + R/I_0 + \epsilon I_0 G_0) + AI_0 G_0\}} \tag{12a}$$

$$\frac{I_2}{I_1} = \frac{1}{2}\frac{(2j\Omega + S_N)(j\Omega + R/I_0 - \epsilon^2 I_0^2 G_0) - (S_{NN}/2A)(j\Omega + R/I_0 + \epsilon I_0 G_0)^2}{\{(2j\Omega + S_N + AI_0)(2j\Omega + R/I_0 + \epsilon I_0 G_0) + AI_0 G_0\}}\frac{I_1}{I_0}. \tag{12b}$$

From (12b), it can immediately be seen that the static (LF) distortion in Fabry–Perot lasers is strongly dependent on the spontaneous carrier recombination via S_N and S_{NN}. Indeed, neither gain suppression nor spontaneous emission alter the external quantum efficiency, which is given by the ratio of the reflection losses and the total losses. The only result of both nonlinearities is that the carrier density and hence the effective threshold current (determined by the spontaneous carrier recombination) change because the effective gain ($= G_0(1 - \epsilon I_0) + R/I_0$) has to compensate the loss. It can also be verified from (12b) that the effect of different nonlinearities cannot simply be superposed. Nevertheless, in many situations, one of the nonlinearities will be dominating and we will therefore often consider each nonlinearity separately. (An exception is made in (4a) where the simultaneous presence of spatial and spectral hole burning is considered.)

Spontaneous emission only has an influence at low bias levels and the gain suppression will dominate at power levels of 1 mW or higher. The distortion caused by gain suppression increases with increasing bias level for a constant optical modulation depth (OMD $= I_1/I_0$). It always has a phase π at low modulation frequencies, i.e., the effective threshold current increases and the external efficiency decreases with increasing injection current.

Numerical calculations of the distortion in a F-P laser are shown in Figs. 2 and 3 for different situations. In these figures, as well as in the following ones, dashed curves belong to the right axis. The laser (FP1) under consideration has a length of 300 μm and both facets have a reflectivity of 80%. This high facet reflectivity guarantees a relative uniform longitudinal distribution of the optical power and hence that spatial hole burning has a negligible influence (as will be shown furtheron). The threshold current is 10.8 mA. The material parameters are listed in Table I. Fig. 2 shows the effect of spontaneous emission at a bias current of 15 mA (corresponding with a static output power of 0.2 mW) for a modulation current of 1 mA. Gain suppression has been neglected here and the distortion induced by spontaneous emission at this relatively low bias level is already extremely small. The relaxation oscillation dominates for modulation frequencies above a few megahertz.

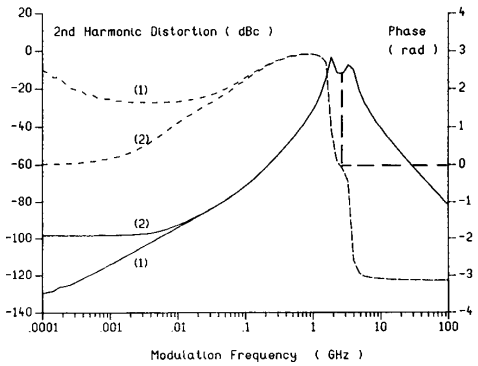

Fig. 2. Distortion of the Fabry–Perot laser FP1 with (2) and without (1) spontaneous emission; the bias current is 15 mA and the modulation current 1 mA. Spectral hole burning is not included. (——): amplitude, (- - -): phase.

The contribution from the relaxation oscillation increases with 20 dBc per decade and, near the resonance peak with 40 dBc per decade. Two resonance peaks appear, but it must be noticed that the second peak is caused by a resonance in the AM response and will not occur if a constant OMD is considered. It can also be noticed that the phase reaches zero just halfway the two resonance peaks. Furthermore, it is also seen that spontaneous emission has no significant influence on the resonance frequency f_0 and on the damping rate Γ (of the first peak) [16], which can be approximated as:

$$(4\pi f_0)^2 = AI_0 G_0 \tag{13a}$$

$$\Gamma = AI_0 + S_N. \tag{13b}$$

The influence of gain suppression is shown in Fig. 3 for different values of ϵ (3, 6 and 11 W^{-1}). The bias cur-

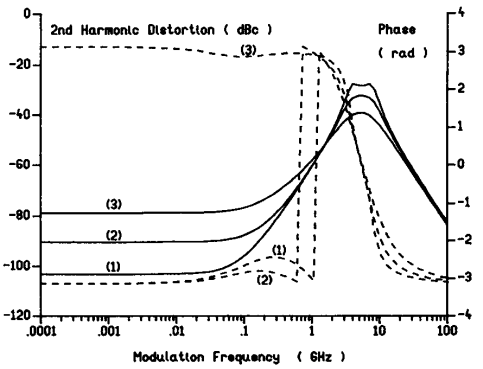

Fig. 3. Distortion of FP1 for different levels of gain suppression: (1) ϵ = 3 W^{-1}, (2) ϵ = 6 W^{-1}, (3) ϵ = 11 W^{-1}; the bias current is 30 mA. (——): amplitude, (- - -): phase.

TABLE I

Parameter	Typical Value	
w [μm]	1.5	Stripe width
d [μm]	0.12	Active layer thickness
L [μm]	300	Laser length
η	0.3	Power confinement factor
Λ [μm]	0.2413	Grating period (for DFB lasers)
n_e	3.25	Unperturbated effective refractive index
v_g [μm/s]	$7.5\ 10^{13}$	Group velocity
α_{int} [μm^{-1}]	$50\ 10^{-4}$	Internal waveguide loss
β_{sp}	10^{-4}	Spontaneous emission factor
τ[s]	$5\ 10^{-9}$	Carrier lifetime
B [μm^3/s]	100	Bimolecular recombination
C [μm^6/s]	$7.5\ 10^{-5}$	Auger recombination

rent is 30 mA and the modulation current is 1 mA. The static distortion is almost bias-independent, as predicted by (12b). The only small bias dependence is due to an increase of S_N and S_{NN} with increasing bias level. If the OMD is kept constant however, the distortion will increase with increasing bias level. Another result of the gain suppression is that now the relaxation peaks are strongly damped. The influence of the gain suppression coefficient ϵ on this damping can be seen from the analytical expression for Γ [13]:

$$\Gamma = AI_0 + S_N + \epsilon I_0 G_0. \tag{14}$$

The increased damping for increasing gain suppression can be seen on Fig. 3. From this figure, it can also be verified that a doubling of ϵ increases the static distortion with 12 dBc, as is predicted by (12b).

The laser, considered before, has relatively high facet reflectivities and the optical power is rather uniform in the longitudinal direction. In Fabry–Perot lasers with a less uniform power distribution, an additional distortion in the AM response can result from the spatial hole burning. The nonlinearity caused by spatial hole burning is explained in more detail in Appendix A where it is shown that, in general, the output power is a nonlinear function of the average photon density. The rate equations must be modified as

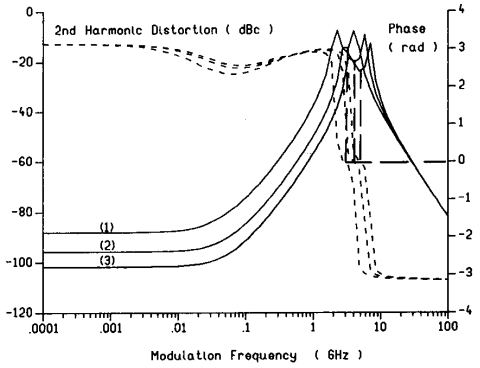

Fig. 4. Influence of spatial hole burning on the distortion of FP2 for a modulation current of 1 mA and for different bias levels: (1) I = 20 mA, P_{out} = 1 mW, (2) I = 25 mA, P_{out} = 1.8 mW, (3) I = 30 mA, P_{out} = 2.7 mW. Spectral hold burning and spontaneous emission are not included. (——): amplitude, (- - -): phase.

$$\frac{dI}{dt} = (G - \Gamma)\, I(1 - \epsilon_{sph} I) + R \tag{15a}$$

$$\frac{dN}{dt} = \frac{J}{q} - S(N) - GI(1 - \epsilon_{sph} I) \tag{15b}$$

with ϵ_{sph} being a decreasing function of power level (see Appendix A) and, in fact, also of modulation frequency. At static frequencies, the distortion can now easily be calculated from the expression (12b) by substituting I by $I(1 - \epsilon_{sph} I)$. In calculating the distortion in the output power, one must of course also take into account the nonlinear relation between the output power and I (see Appendix A):

$$P_{out} \sim \{(AN - B)\,(1 - \epsilon_{sph} I) I - \alpha_{int} v_g I\}. \tag{16}$$

This spatial hole burning effect is illustrated in Fig. 4 for a 300 μm long F–P laser with cleaved (R = 30%) facets (FP2). The threshold current is now 14.3 mA. The modulation current is again 1 mA and all other static nonlinearities have been neglected in the calculation of the distortion. As can be seen, the distortion caused by the spatial hole burning in Fabry–Perot lasers has a phase π, which agrees with the following simple expression that can be derived from (15) and (16):

$$\frac{P_{out,2}}{P_{out,1}} = \frac{-\alpha_{int} L \epsilon_{sph} I_1}{\ln\left(\dfrac{1}{R_1 R_2}\right)}. \tag{17}$$

The value of ϵ_{sph} is strongly dependent on the facet reflectivities. Table II gives values of ϵ_{sph} (calculated at threshold) for a 300 μm long Fabry–Perot laser as a function of $R = R_1 = R_2$. From these values, it follows that the spatial hole burning induced distortion in laser FP1 is about 40 dB lower than that of laser FP2. For cleaved or HR-coated facets, the distortion caused by this spatial hole burning nonlinearity will be much weaker than the one

TABLE II

Facet Power Reflectivity	Gain Suppression ϵ_{shb} [W^{-1}]
0.05	19.015
0.1	8.578
0.2	2.585
0.3	0.915
0.4	0.3325
0.5	0.11536
0.6	0.03558
0.7	$8.762\ 10^{-3}$
0.8	$1.382\ 10^{-3}$
0.9	$7\ 10^{-5}$
1	0

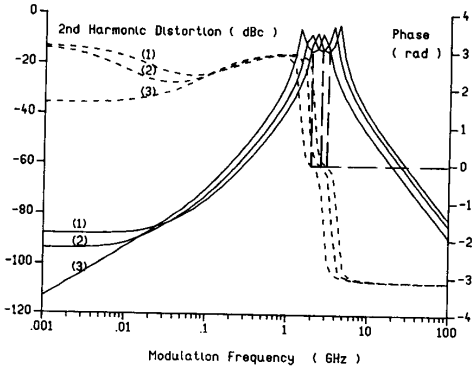

Fig. 5. Influence of the internal absorption on the spatial hole burning induced distortion of FP2: (1) $\alpha_{int} = 50\ cm^{-1}$, (2) $\alpha_{int} = 25\ cm^{-1}$, and (3) $\alpha_{int} = 0\ cm^{-1}$. The static output power is 1 mW and the optical modulation depth (OMD) is 20%. Spectral hole burning and spontaneous emission are not included. (——): amplitude, (– – –): phase.

caused by the gain suppression, but the effect can become important for lower facet reflectivities.

The spatial hole burning induced distortion is also strongly dependent on the internal absorption. This is illustrated in Fig. 5 where the distortion for several values of the internal absorption is depicted. The distortion is however not proportional to the internal absorption since ϵ_{sph} is also dependent on the carrier lifetime, which generally increases with decreasing absorption.

We conclude this section by mentioning that gain suppression, spontaneous emission, and relaxation oscillations have similar effects on Fabry–Perot and DFB lasers. From the previous results, it follows that spontaneous emission can be neglected already at low power levels and that the distortion caused by gain suppression and/or relaxation oscillations can be well described by the analytical formula (12b) and has a phase π.

IV. Distortion in DFB Lasers

The effect of spontaneous emission, gain suppression, and relaxation oscillations on the distortion in DFB laser is very similar to the case of Fabry–Perot lasers. Longitudinal spatial hole burning, however, is far more important in DFB lasers and therefore we will concentrate on

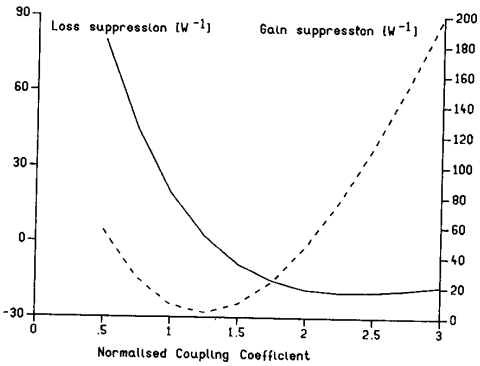

Fig. 6. Variation of the loss suppression ($\epsilon_{s,2}$) and the gain suppression ($\epsilon_{s,1}$), caused by spatial hole burning in $\lambda/4$-shifted DFB-lasers, as a function of κL ($L = 300\ \mu m$).

the distortion caused by this spatial hole burning and its combination with other nonlinearities. We only consider DFB lasers that are single mode up to high power levels.

First, an analytical approach is given for an important class of DFB lasers, namely AR-coated DFB lasers which emit at the Bragg wavelength and where the power is symmetric with respect to $z = L/2$. The spatial hole burning in such lasers can easily be approximated in an analytical way. However, such an analytical approach is very hard (if not impossible) for other DFB lasers. We therefore also include modeling results for a DFB laser with one cleaved and one AR-coated facet.

A. DFB Lasers Emitting at the Bragg Wavelength

For lasers where the main mode lases at the Bragg wavelength and is symmetric with respect to $z = L/2$, such as $\lambda/4$-shifted lasers, the effect of spatial hole burning on the distortion is mainly due to the longitudinal nonuniformity of the gain. The nonuniformity of the refractive index is of little importance in such lasers. The gain and loss that must then be used in the rate equation can, according to Appendixes A and B be written as

$$G = (AN - B)(1 - \epsilon_{s,1} I) \tag{18a}$$

$$\Gamma = \Gamma_m + \Gamma_a = \Gamma_{m,o}(1 - \epsilon_{s,2} I) + \Gamma_a \tag{18b}$$

with Γ_m being the power dependent mirror losses and Γ_a the constant absorption losses. $\epsilon_{s,1}$ and $\epsilon_{s,2}$ represent the gain and loss suppression (Fig. 6) due to spatial hole burning and $\epsilon_{s,1}$ has the same definition as ϵ_{sph} for Fabry–Perot lasers. Both $\epsilon_{s,1}$ and $\epsilon_{s,2}$ decrease with increasing power level and $\epsilon_{s,2}$ can be either positive or negative. Since the output power can be written as

$$P_{out} \sim I(1 - \epsilon_{s,2} I) = P \tag{19}$$

it is convenient to transform the rate equations. In the absence of spontaneous emission and gain suppression and for low modulation frequencies one finds

$$(AN - B)(1 - \Delta\epsilon P) = \Gamma_{m,o} + \Gamma_a(1 + \epsilon_{s,2} P) \tag{20a}$$

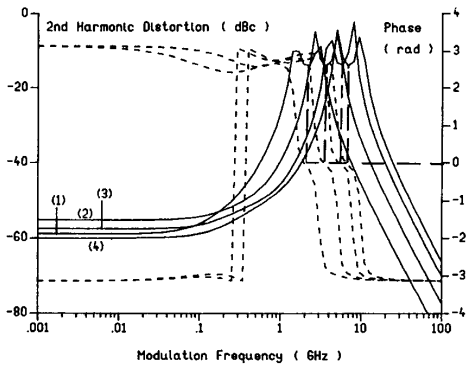

Fig. 7. Distortion in the case $\epsilon = 0$ for a $\lambda/4$-shifted laser with $\kappa L = 1$, $L = 300$ μm and for an OMD of 20%: (1) $I = 25$ mA, (2) $I = 30$ mA, (3) $I = 40$ mA, (4) $I = 50$ mA. (——): amplitude, (- - -): phase.

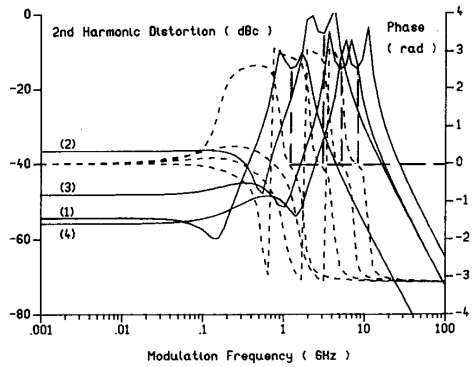

Fig. 8. Distortion in the case $\epsilon = 0$ for a $\lambda/4$-shifted laser with $\kappa L = 2$, $L = 300$ μm and for an OMD of 20%: (1) $I = 16$ mA, (2) $I = 20$ mA, (3) $I = 30$ mA, (4) $I = 50$ mA. (——): amplitude, (- - -): phase.

$$\frac{J}{q} = S(N) + (AN - B)\,P(1 - \Delta\epsilon P) \qquad (20b)$$

with $\Delta\epsilon = \epsilon_{s,1} - \epsilon_{s,2}$. In the case that also gain suppression (characterized by ϵ) is included, one has $\Delta\epsilon = \epsilon_{s,1} - \epsilon_{s,2} + \epsilon$. Fig. 7 shows the variation of $\epsilon_{s,1}$ and $\epsilon_{s,2}$ (calculated at threshold) for 300 μm long, $\lambda/4$-shifted DFB lasers as a function of κL. $\epsilon_{s,1}$ and $\epsilon_{s,2}$ take a minimum value for $\kappa L \approx 1.25$, a value which is known to give minimum spatial hole burning in $\lambda/4$-shifted lasers [17]. It can also be remarked that $\epsilon_{s,1}$ and $\epsilon_{s,2}$ can be calculated by a laser model in which spatial hole burning is not taken into account.

From a small signal solution of the equations in (20), one finds for the low frequency second-hamonic distortion in the AM response

$$\frac{P_{\text{out},2}}{P_{\text{out},1}} = -\frac{1}{2}\,\frac{A\Gamma_a\epsilon_{s,2}I_0^2 + S_N\Delta\epsilon I_0^2(\epsilon_{s,2}\Gamma_a + \Delta\epsilon G_0) + \dfrac{S_{\text{NN}}}{2A}I_0^2(\epsilon_{s,2}\Gamma_a + \Delta\epsilon G_0)^2}{AG_0I_0 + (S_N + AI_0)\epsilon_{s,2}\Gamma_aI_0 + \Delta\epsilon G_0S_NI_0}\,\frac{P_{\text{out},1}}{P_{\text{out},0}}. \qquad (21)$$

$\epsilon_{s,2}\Gamma_a$ and $\Delta\epsilon G_0$ are of the same order of magnitude in this expression, while $\Delta\epsilon S_N \ll A$ and $\epsilon_{s,2}S_{\text{NN}}\Gamma_a \ll A^2$. The first term in the denominator of (21) is therefore dominant at low power levels, except for κL values in the neighborhood of 1.25. It must further be noted that $\epsilon_{s,1}$ and $\epsilon_{s,2}$ have been considered as power independent in the derivation of formula (21). The actual power dependence of $\epsilon_{s,1}$ and $\epsilon_{s,2}$ can not easily be calculated above threshold, but this power dependence will certainly result in additional distortion.

The spatial hole burning effect is illustrated in Fig. 7, resp. Fig. 8 for 300 μm long, $\lambda/4$-shifted DFB-lasers with $\kappa L = 1$ (and a threshold current of 22.5 mA), resp. $\kappa L = 2$ (and a threshold current of 15 mA). These results are obtained with the longitudinal model, but they agree very well with the analytical results. As can be seen, the low frequency AM distortion has a phase π for $\kappa L = 1$ and a phase 0 for $\kappa L = 2$, which agrees with expression (21). Indeed, in the limit of low power levels, one finds $\epsilon_{s,1} = 8.35$ W^{-1} and $\epsilon_{s,2} = 19.4$ W^{-1} for $\kappa L = 1$ and $\epsilon_{s,1} = 47.4$ W^{-1} and $\epsilon_{s,2} = -18.9$ W^{-1} for $\kappa L = 2$. Also according to expression (21), the amplitude of the static distortion increases with the bias level for a constant optical modulation depth. In Figs. 7 and 8, this behavior is seen only at low bias levels and at high bias levels the spatial hole burning induced distortion decreases monotonically with bias level. This discrepancy can be attributed to our small signal approximation (as given in Appendix B) of spatial hole burning, which does not produce the exact bias dependence of $\epsilon_{s,2}$.

The level of distortion depends not only on the spatial hole burning (expressed by $\epsilon_{s,2}$) and on the bias level, but also on the ratio of internal (absorption) loss and external (mirror) loss. More specific, the amplitude of the distortion decreases with increasing external loss (i.e., decreasing κL-value). It can furthermore be noticed that for decreasing κL values a smaller number of photons in the cavity corresponds to a certain output power level. As a result, lower κL values will in general result in less distortion, as far as the κL dependence of $\epsilon_{s,2}$ is not considered. For example, the magnitude of $\epsilon_{s,2}$ is almost the same for $\kappa L = 1$ and $\kappa L = 2$, but the distortion level is approximately 10 dBc lower for $\kappa L = 1$, due to the larger mirror loss (or threshold gain). Equivalently, a reduction of the absorption losses could bring about a similar reduction in the static distortion. This can also easily be seen after substitution of the gain, which equals the total loss, in the static carrier rate equation:

$$\frac{J}{q} = S(\mathfrak{N}) + \Gamma_{m,o}(1 - \epsilon_{s,2}I)I + \Gamma_aI. \qquad (22)$$

For small absorption losses and since the mirror loss is proportional to the output power, the only nonlinearity is due to a power dependence of the carrier density (and hence of S).

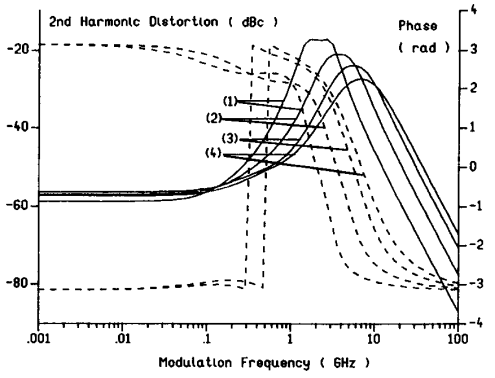

Fig. 9. Distortion when $\epsilon = 11\ W^{-1}$ for a $\lambda/4$-shifted laser with $\kappa L = 1$, $L = 300\ \mu m$ and for an OMD of 20%: (1) $I = 25$ mA, (2) $I = 30$ mA, (3) $I = 40$ mA, (4) $I = 50$ mA. (———): amplitude, (- - -): phase.

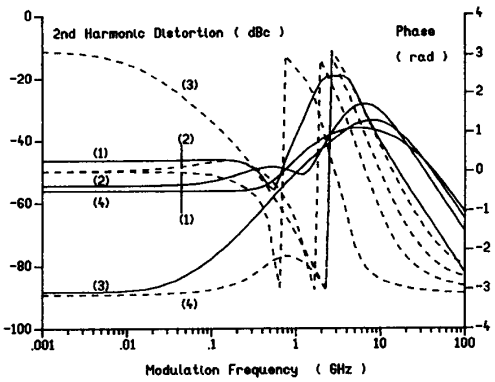

Fig. 10. Distortion caused when $\epsilon = 11\ W^{-1}$ for a 300 μ long $\lambda/4$-shifted laser with $\kappa L = 2$ and for an OMD of 20%: (1) $I = 20$ mA, (2) $I = 40$ mA, (3) $I = 60$ mA, (4) $I = 80$ mA. (———): amplitude, (- - -): phase.

At modulation frequencies of 100 MHz or more, a relaxation oscillation contribution (consisting of a term with phase $\pi/2$ and a term with phase π) interferes with the spatial hole burning contribution. At the same time, the spatial hole burning contribution starts to roll off. Destructive interference with a spatial hole burning contribution with phase 0 can then result in the occurrence of a dip as in Fig. 8. With increasing bias level, this dip occurs at higher modulation frequencies since the relaxation oscillation and the roll-off of the spatial hole burning start at higher frequencies. Obviously, such a dip is more or less desirable, since it keeps or makes the distortion low at high modulation frequencies.

Figs. 9 and 10 show the second-harmonic distortion for both $\lambda/4$-shifted lasers when gain suppression is also taken into account. As has already been mentioned, this gain suppression can be accounted for by including the gain suppression coefficient ϵ_0 in $\Delta\epsilon$. Comparison of a typical value $\epsilon_0 = 11\ W^{-1}$ with $\epsilon_{s,1}$ and $\epsilon_{s,2}$ shows that the gain suppression will often be less important than the spatial hole burning, at least at low bias levels. However, the spatial hole burning induced distortion decreases rapidly at higher bias levels, while the gain suppression contribution (which always has a phase π) increases with bias level (ϵ_0 is practically independent of the bias level). In Fig. 9, this dominance of gain suppression at high bias levels can be seen as an increase in distortion amplitude with bias level for bias currents of 50 mA or more.

A more pronounced effect of the combination of spatial hole burning and gain suppression can be seen in Fig. 10. For $\kappa L = 2$, both contributions (with phases 0, resp. π) will interfere destructively and at a certain bias level where they have equal amplitude, they can cancel each other. This gives rise to a dip in the bias dependence of the static distortion. Beyond the dip, the gain suppression becomes dominant, the phase equals π and the distortion increases with bias level. At this point, $\epsilon_{s,1}$ and $\epsilon_{s,2}$ are becoming less important and the distortion is determined by the terms in $\Delta\epsilon^2$ (which itself is determined by ϵ_0) in formula (21). The dip in the frequency dependence of the distortion then also disappears. In Fig. 9, the dip occurs at relatively high bias level due to the strong spatial hole burning for κL values of 2 or more. For κL values closer to 1.25, the dip can be expected to occur at lower bias levels.

B. Other DFB-Lasers

Most DFB lasers are not of the former type, e.g., lasers without phase shifts and with one or two partly reflecting facets. Such lasers do not emit at the Bragg wavelength and in general the optical power distribution will not be symmetric. The effect of longitudinal spatial hole burning can then no longer be calculated in a similar, easy way as described in Appendix B for $\lambda/4$-shifted lasers. Moreover, the effect is not solely due to the nonuniform gain. The nonuniformity of the refractive index (and hence of the real part of the Bragg deviation) may be equally or more important. An analytical treatment of the spatial hole burning effect seems to be very complicated. Therefore, we will only give a brief overview of the modelling results that were found for other laser types.

For all the lasers we investigated so far, the spatial hole burning induced distortion decreases with bias level at moderate and high bias levels. This behavior is quite general. The spatial hole burning induced distortion gain can have either a phase 0 or a phase π, depending on the κL value and on the lasertype. Still, a phase 0 (π) will rather result for high (low) κL values. A dip in the frequency dependence and in the bias dependence of the distortion can be observed if the spatial hole burning induced distortion has a phase 0. Hence, in general the same effects as in $\lambda/4$-shifted lasers occur, despite the fact that the spatial hole burning mechanism is more complex.

In theory, the influence of spatial hole burning in such lasers can still be represented by a power dependence of gain and loss. A formula such as (22) will still be valid and it can be expected that the distortion decreases with decreasing internal absorption. A roll-off of the spatial hole burning always occurs around 1 GHz and therefore spatial hole burning has only a minor influence on the re-

laxation oscillation peak. The damping of this peak is mainly due to gain suppression and is not different from Fabry–Perot lasers.

IV. Conclusion

Detailed calculations of the second-harmonic distortion in the AM response of Fabry–Perot and DFB lasers have been discussed. Modulation frequencies ranging from 1 MHz to more than 10 GHz have been considered and several nonlinearities such as spatial hole burning, gain suppression, spontaneous emission, and relaxation oscillations have been taken into account. A few effects such as the presence of leakage currents and the fact that the absorption generally depends on the carrier density have been ignored in this study. Since the values of the distortion found in this study and of the leakage-current induced distortion [11] may seem a little low as compared to experimental values, it follows that both the effects considered here and the leakage currents [11] should be taken into account to obtain better agreement between theoretical and experimental values. In this paper we mainly tried to clarify the influence of gain suppression and spatial hole burning.

The main reason for the investigation of Fabry–Perot lasers is that, when the facet reflectivities are not too small, spatial hole burning has no significant influence in this case and therefore the relative importance of gain suppression, spontaneous emission, and relaxation oscillations can be easily determined. However, DFB lasers are far more important from a practical point of view and their nonlinear behavior forms the main subject of this paper.

In particular the spatial hole burning induced distortion in DFB lasers has been clarified. It was shown that this distortion can either have a phase 0 or a phase π, depending on the lasertype. A distortion with phase 0, which is generally the case for κL more than 1–1.5, interferes destructively with the distortion caused by the relaxation oscillation, resulting in a dip (and hence a low distortion) at a modulation frequency around 1 GHz. For AR-coated lasers which emit at the Bragg wavelength (e.g., $\lambda/4$-shifted lasers), an analytical formula is given which allows to calculate the spatial hole burning induced distortion from the longitudinal variation of the power (calculated, e.g., without taking spatial hole burning into account). Our analytical treatment, however, cannot explain the decrease of the spatial hole burning induced distortion at higher bias levels. It can not be extended to DFB lasers with a more complex behavior, for which the longitudinal model had to be used.

The distortion caused by gain suppression always has a phase π and increases with the bias level. If the spatial hole burning induced distortion, which decreases with bias level (except at low bias levels), has a phase 0 then the two contributions can cancel each other at some specific bias level, giving rise to a dip in the bias dependence of the static distortion. The distortion caused by gain suppression strongly depends on the electron lifetime and on the gain suppression coefficient.

A few guidelines for reduction of the distortion can be derived from our study. The spatial hole burning induced distortion can be minimized by using a κL value between 1 and 1.5 (depending on the laser structure), but also by increasing the efficiency (i.e., decreasing the absorption or increasing the mirror loss). Furthermore, a spatial hole burning induced distortion with a phase 0 must be pursued. The destructive interference with the relaxation oscillation contribution then keeps the distortion low for modulation frequencies up to about 1 GHz, while the destructive interference with the gain suppression contribution also results in reduced static distortion for small range of bias levels. A spatial hole burning contribution with a phase 0 can for most laser structures be obtained by using a κL value in the neighborhood of 1.5 rather than a κL value in the neighborhood of 1.

The presented study is currently being extended to the third-order harmonic distortion, for which a similar numerical approach can be used.

Appendix A
Longitudinal Spatial Hole Burning in Fabry–Perot Lasers

The implications of a longitudinally nonuniform power (or photon density) follow, for a Fabry-Perot laser from the carrier rate equation. We assume that the photon density $P(z)$ can be written as

$$P(z) = P_0(1 + f(z)) \tag{A1}$$

with f being a function that is smaller than unity and for which

$$\int_0^L f(z)\, dz = 0. \tag{A2}$$

The resulting nonuniform carrier density $N(z, t)$ can be expanded to first order in f as

$$N(z, t) = N_0(t) + N_1(t) f(z). \tag{A3}$$

N_1 can be assumed to be much smaller than N_0 (at least at moderate power levels). Substitution of (A1) and (A3) in the carrier density rate equation:

$$\frac{\partial N}{\partial t} = \frac{J}{qd} - \frac{N}{\tau} - \mathrm{BN}^2 - \mathrm{CN}^2 - (\mathrm{AN} - B)\, P(z) \tag{A4}$$

allows to determine both N_1 and N_0. After linearization, one finds the following equation for N_1:

$$\frac{\partial N_1}{\partial t} + N_1\left\{\frac{1}{\tau} + 2\mathrm{BN}_0 + 3\mathrm{CN}_0^2 + \mathrm{AP}_0\right\} = -(\mathrm{AN}_0 - B)P_0 \tag{A5}$$

for static frequencies, it follows immediately:

$$N_1 = -\frac{(AN_0 - B)P_0}{\frac{1}{\tau} + 2BN_0 + 3CN_0^2 + AP_0} = -\frac{(AN_0 - B)P_0}{\frac{1}{\tau'} + AP_0}. \tag{A6}$$

The rate equation for N_0 can then be tranformed into

$$\frac{J}{qd} = \frac{N_0}{\tau} + BN_0^2 + CN_0^3 + (AN_0 - B)P_0 \cdot \left\{ 1 - \frac{\frac{1}{L}\int_0^L f^2\, dz\, AP_0}{\frac{1}{\tau'} + AP_0} \right\}. \tag{A7}$$

Spatial hole burning thus results in a gain reduction.

A different approach must be used for the photon rate equation. We will show that in the absence of gain suppression (e.g., spectral hole burning) and spontaneous emission and for a Fabry–Perot laser, N_0 is still clamped (and determined by the constant loss), but that the output power P [proportional with $P^+(L)$ or $P^-(0)$] is a nonlinear function of the average photon density P_0. We start from the amplitude rate equations (formula 3, Section II), which can be transformed into the equations for the photon densities P^+ and P^- of forward and backward propagating waves:

$$\frac{\partial P^+}{\partial t} + v_g \frac{\partial P^+}{\partial z} = (G - \alpha_{int} v_g)P^+ \tag{A8a}$$

$$\frac{\partial P^-}{\partial t} - v_g \frac{\partial P^-}{\partial z} = (G - \alpha_{int} v_g)P^-. \tag{A8b}$$

For low frequencies, one can derive the longitudinal variation of P^+ and P^- from these equations, giving

$$P^+(z) = P^+(0) \exp\left[\int_0^z (g - \alpha_{int})\, dz\right] \tag{A9a}$$

$$P^-(z) = P^-(L) \exp\left[\int_z^L (g - \alpha_{int})\, dz\right] \tag{A9b}$$

with $g = G/v_g$. Substitution of (A9) in the boundary conditions, $P^+(0) = R_1 P^-(0)$ and $P^-(L) = R_2 P^+(L)$, results in the oscillation condition, from which the clamping of N_0 follows:

$$AN_0 - B - v_g\alpha_{int} = \frac{v_g}{2L} \ln\left(\frac{1}{R_1 R_2}\right). \tag{A10}$$

Since N_0 determines the FM response, it follows already that this nonlinearity does not give a contribution to the FM. The sum of forward and backward propagating photon densities can be expressed as (with $a = A/v_g$ and $b = B/v_g$)

$$P(z) = P^+(0)\left[e^{(aN_0 - b - \alpha_{int})z} + \frac{1}{R_1} e^{-(aN_0 - b - \alpha_{int})z}\right] + P^+(0)\left[e^{(aN_0 - b - \alpha_{int})z} - \frac{1}{R_1} e^{-(aN_0 - b - \alpha_{int})z}\right] \cdot aN_1 \int_0^z f dz. \tag{A11}$$

In deriving this expression, it has been assumed that N_1 is small and hence

$$\exp\left\{aN_1 \int_0^z f dz\right\} = 1 + aN_1 \int_0^z f dz. \tag{A12}$$

Equation (A11), with the left-hand side being equal to $P_0(1 + f)$, is an integral equation for f and can in theory be solved by well-known perturbation methods. Integration of (A11) gives an expression for P_0:

$$LP_0 = \frac{P^+(0)}{aN_0 - b - \alpha_{int}}\left\{e^{-(aN_0 - b - \alpha_{int})L} - 1 + \frac{1}{R_1} - \frac{1}{R_1} e^{-(aN_0 - b - \alpha_{int})L}\right\} - \frac{aN_1 P^+(0)}{aN_0 - b - \alpha_{int}} \int_0^L f\left\{e^{+(aN_0 - b - \alpha_{int})z} + \frac{1}{R_1} e^{-(aN_0 - b - \alpha_{int})z}\right\} dz. \tag{A13}$$

It must now be noticed that the part of the integrand between brackets can be approximated, from (A11), as $P_0(1 + f)/P^+(0)$. When the threshold condition (A10) is also taken into account, one finds the following relation between P_0 and $P^+(0)$:

$$\left[(AN_0 - B)\left(1 - \frac{AP_0 \frac{1}{L}\int_0^L f^2\, dz}{\frac{1}{\tau'} + AP_0}\right) - \alpha_{int} v_g\right] P_0 = [(AN_0 - B)(1 - \epsilon_{sph} P_0) - \alpha_{int} v_g] P_0 = \frac{P^+(0) v_g}{L} \frac{[1 - \sqrt{R_1 R_2}]}{R_1}\left(1 + \sqrt{\frac{R_1}{R_2}}\right) \tag{A14}$$

which proves that the output power [proportional with $P^+(0)$] is a nonlinear function of the average photon density P_0 or of the total photon number $I = P_0 L$. ϵ_{sph} as defined in (A14) has the dimension (cm). Naturally, it is also possible to use the average power level inside the cavity instead or the photon number, in which case ϵ_{sph} has the dimension $[W^{-1}]$ or, in the second case, is dimensionless.

The nonlinearity expressed by (A7) and (A17) causes additional distortion in the AM response of F–P lasers. It must be noticed that the nonlinear relation between P_0 and

$P^+(0)$ also implies that the gain and mirror losses, to be used in a rate equation for P_0, become power dependent.

Appendix B
Spatial Hole Burning in $\lambda/4$-Shifted DFB-Lasers

For DFB lasers, it can also be shown that the output power is a nonlinear function of the average photon density due to a longitudinal variation in the gain. We will neglect the longitudinal variation of the refractive index, which means that phase variations caused by the spatial hole burning are not taken into account in the amplitude equations. This approach is correct for lasermodes at the Bragg wavelength (as in $\lambda/4$-shifted lasers), in other cases it means that only part of the spatial hole burning effect is considered. Again we assume that the photon density $P(z)$ can be written as

$$P(z) = P_0(1 + f(z)). \tag{B1}$$

The rate equation for the carrier density N_0 is then identical to the one of Appendix A and a similar gain reduction can be used.

The nonlinear relation between average photon density and output power can be derived from the static amplitude rate equations, which are

$$\frac{\partial r^+}{\partial z} - \Delta\beta_i r^+ = \kappa r^- \cos(\phi_\kappa + \phi^- - \phi^+) \tag{B2a}$$

$$-\frac{\partial r^-}{\partial z} - \Delta\beta_i r^- = -\kappa r^+ \cos(\phi_\kappa + \phi^- - \phi^+). \tag{B2b}$$

The nonuniform carrier density implies that $\Delta\beta_i$ can be written as

$$\Delta\beta_i = \Delta\beta_{i0} + \Delta\beta_{i1} f \tag{B3}$$

with

$$\Delta\beta_{i1} = \frac{AN_1}{2v_g}. \tag{B4}$$

From the coupled wave equations (B2), the following wave equation for r^+ and r^- can be derived:

$$\frac{\partial^2 r^\pm}{\partial z^2} = \left(\Delta\beta_{io}^2 + \kappa^2 \cos^2(\phi_\kappa + \phi^- - \phi^+) + 2\Delta\beta_{io}\Delta\beta_{i1} f \pm \Delta\beta_{i1}\frac{\partial f}{\partial z}\right) r^\pm. \tag{B5}$$

We now decompose the fields r^+ and r^-, corresponding with the nonuniform Bragg deviation as

$$r^\pm = r_0^\pm(1 + F^\pm) \tag{B6}$$

with $r_0^\pm(z)$ being the fields corresponding with $\Delta\beta_{i0}$. Substitution of (B6) in (B5) allows to determine $F^\pm$ and one finds

$$\frac{\partial F^\pm}{\partial z} = \pm\Delta\beta_{i1}\left[f(z) - \frac{2\kappa}{(r_0^\pm)^2}\int_0^z dz' f(z') r_0^+ r_0^- \cdot \cos(\phi_\kappa + \phi^- - \phi^+)\right] = \pm\Delta\beta_{i1}\left[f(z) - \frac{2\kappa}{(r_0^\pm)^2}\delta(z)\right]. \tag{B7}$$

After integration of (B7), the fields can be determined. Assumption of the boundary conditions $r^+(L) = r_0^+(L)$ and $r^-(0) = r_0^-(0)$, gives

$$F^+ = \Delta\beta_{i1}\int_0^z f(z')\,dz' - 2\kappa\Delta\beta_{i1}\int_L^z dz' \frac{\delta(z')}{(r_0^+(z'))^2} \tag{B8a}$$

$$F^- = \Delta\beta_{i1}\int_0^z f(z')\,dz' + 2\kappa\Delta\beta_{i1}\int_0^z dz' \frac{\delta(z')}{(r_0^-(z'))^2}. \tag{B8b}$$

For the photon density $P(z)$ one finds, after appropriate normalization of $r_0^\pm$,

$$P(z) = (r_0^+)^2 + (r_0^-)^2 + 2\Delta\beta_{i1}[(r_0^+)^2 - (r_0^-)^2] \cdot \int_0^z dz' f(z') + 4\kappa\Delta\beta_{i1}\left[(r_0^+)^2\int_z^L dz' \frac{\delta(z')}{(r_0^+)^2} + (r_0^-)^2\frac{\delta(z')}{(r_0^-)^2}\right]. \tag{B9}$$

Calculation of the average photon density gives

$$P_0 = \frac{1}{L}\int_0^L [(r_0^+)^2 + (r_0^-)^2]\,dz - 2\Delta\beta_{i1}\frac{1}{L}\int_0^L \cdot dz\, f(z)\int_0^z [(r_0^+)^2 - (r_0^-)^2]\,dz + 4\kappa\frac{\Delta\beta_{i1}}{L}\int_0^L dz\left[(r_0^+)^2\int_z^L dz'\frac{\delta(z')}{(r_0^+)^2} + (r_0^-)^2\int_0^z dz\frac{\delta(z')}{(r_0^-)^2}\right]. \tag{B10}$$

The last term of the right-hand side of (B10) can, after partial integration, be transformed to

$$4\kappa\frac{\Delta\beta_{i1}}{L}\int_0^L dz\,\delta(z)\left[\frac{1}{(r_0^+(z))^2}\int_0^z dz'\,(r_0^+(z'))^2 - \frac{1}{(r_0^-(z))^2}\int_L^z dz'\,(r_0^-(z'))^2\right]. \tag{B11}$$

For $\lambda/4$-shifted lasers, it follows from numerical calculations that this term can be neglected with respect to the other terms in (B10). We shall therefore leave it out here, although it must be noticed that this term is still easily

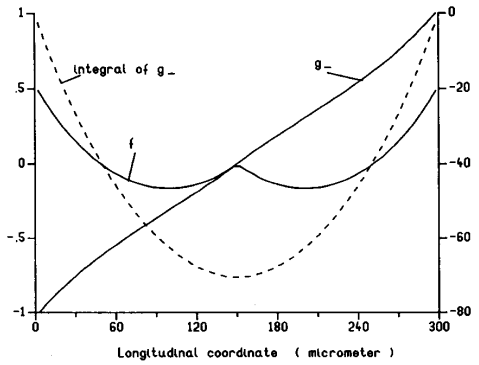

Fig. 11. The functions f, g_-, and the integral of g_- (in microns) for a $\lambda/4$-shifted DFB laser with $\kappa L = 1$.

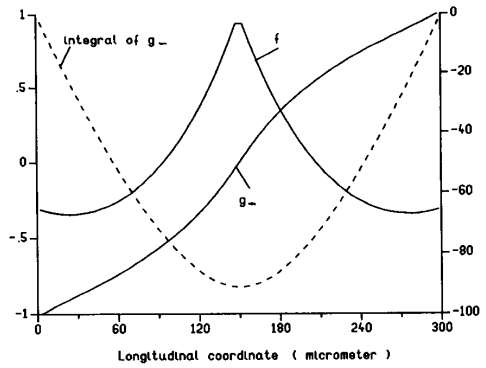

Fig. 12. The functions f, g_-, and the integral of g_- (in microns) for a $\lambda/4$-shifted DFB laser with $\kappa L = 2$.

calculated numerically from a threshold solution. It can also be remarked that, as a result of the assumed boundary conditions, the output power [proportional with $P^-(0)$ or $P^+(L)$] is determined by $r_0^{\pm}$ only, and one can write

$$(r_0^+)^2 + (r_0^-)^2 = P^-(0)\, g_+(z) \qquad \text{(B12a)}$$

$$(r_0^+)^2 - (r_0^-)^2 = P^-(0)\, g_-(z) \qquad \text{(B12b)}$$

with g_+ and g_- being independent of the power level. g_+ and g_- can be obtained from the longitudinal power variation in the absence of spatial hole burning (e.g., calculated at threshold). Equation (B10) can now be transformed into

$$P_0 = P^-(0)\left[\frac{1}{L}\int_0^L g_+(z)\,dz - 2\Delta\beta_{il}\frac{1}{L}\int_0^L \cdot\, dz\, f(z)\int_0^z g_-(z')\,dz'\right] \qquad \text{(B13)}$$

After substitution of the expression for $\Delta\beta_{il}$ [using (A6) and (B4)], one finally finds

$$\frac{1}{L}\int_0^L g_+(z)\,dz\,P^-(0) = \frac{P_0}{1 + \dfrac{(AN_0 - B)\,AP_0\displaystyle\int_0^L dz\, f(z)\int_0^z dz'\, g_-(z')}{v_g\left(\dfrac{1}{\tau'} + AP_0\right)\displaystyle\int_0^L g_+(z)\,dz}}$$

$$= P_0(1 - \epsilon_{s,2}P_0) \qquad \text{(B14)}$$

with the second expression being a quadratic approximation of the first. Again, $\epsilon_{s,2}$ as defined here has the dimension (cm), but when the average power level or the total number of photons inside the cavity is used, the dimension changes as in Appendix A. This formula is valid for all AR-coated lasers which emit at the Bragg wavelength and where the power distribution is symmetric, e.g., also for some multiple phase shifted lasers. The

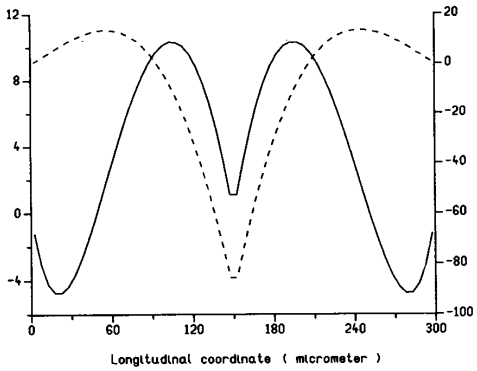

Fig. 13. Product of f and the integral of g_- (in microns) for $\lambda/4$-shifted DFB lasers with $\kappa L = 1$ (——) and $\kappa L = 2$ (- - -).

functions f, g_+, and g_- can, for a given DFB laser, be calculated analytically or numerically. They are depicted in Figs. 11–13 for two AR-coated $\lambda/4$-shifted DFB lasers with $\kappa L = 1$ and $\kappa L = 2$. Fig. 11 shows the functions f, g_-, and the integral of g_- for the case $\kappa L = 1$ and Fig. 12 for the case $\kappa L = 2$. Fig. 13 shows the product of f and the integral of g_- for both cases. From this last figure, it can be concluded that the losses will increase, resp. decrease with increasing power level for $\kappa L = 1$, resp. $\kappa L = 2$.

Again, the gain and loss, to be used in a rate equation for P_0 become power dependent due to this spatial hole burning. However, the power dependence of gain and loss is no longer the same, as is the case in F–P lasers.

References

[1] P. Vankwikelberge, G. Morthier, and R. Baets: "CLADISS, a longitudinal, multimode model for the analysis of the static, dynamic and stochastic behavior of diode lasers with distributed feedback," *IEEE J. Quantum Electron.*, vol. 26, pp. 1728–1741, Oct. 1990.

[2] P. Vankwikelberge, F. Buytaert, A. Franchois, R. Baets, P. Kuindersma, and C. W. Fredriksz," Analysis of the carrier-induced FM-response of DFB lasers: Theoretical and experimental case studies," *IEEE J. Quantum Electron.*, vol. 25, pp. 2239–2254, 1989.

[3] W. I. Way, "Subcarrier multiplexed lightwave system design consid-

erations for subscriber loop applications," *J. Lightwave Technol.*, pp. 1806–1818, 1989.
[4] R. Olshansky, "Subcarrier multiplexed lightwave systems for broadband distribution," *J. Lightwave Technol.*, pp. 1429–1431, 1989.
[5] K. Stubkjaer and M. Danielsen, "Nonlinearities of GaAlAs lasers-harmonic distortion," *IEEE J. Quantum Electron.*, vol. QE-16, pp. 531–537, May 1980.
[6] K. Y. Lau and A. Yariv, "Intermodulation distortion in a directly modulated semiconductor injection lasers," *Appl. Phys. Lett.*, vol. 45, pp. 1034–1036, Nov. 1984.
[7] M. Maeda, K. Nagano, and K. Saito, "Harmonic distortion in semiconductor injection lasers," in *Proc. ECOC.*
[8] T. E. Darcie and R. S. Tucker, "Intermodulation and harmonic distortion in InGaAsP lasers," *Electron. Lett.*, vol. 21, pp. 665–666, Aug. 1985.
[9] A. Takemoto, H. Watanabe, Y. Nakajima, Y. Sakakibara, S. Kakimoto, and H. Namizaki, "Low harmonic distortion distributed feedback laser diode and module for CATV systems," in *Proc. OFC'90*, 1990, p. 214.
[10] M. S. Lin, S. J. Wang, and N. K. Dutta, "Frequency dependence of the harmonic distortion in InGaAsP distributed feedback lasers," in *Proc. OFC'90*, p. 213.
[11] ——, "Measurements and modeling of the harmonic distortion in InGaAsP distributed feedback lasers," *IEEE J. Quantum Electron.*, vol. 26, pp. 998–1004, 1990.
[12] M. Schubert and B. Wilhelmi, *Nonlinear Optics and Quantum Electronics*. New York: Wiley, ch. 1, section 1.4.2, 1986.
[13] A. Yariv, "Coupled-mode theory for guided-wave optics," *IEEE J. Quantum Electron.*, vol. QE-9, pp. 919–933, Sept. 1973.
[14] M. Asada and Y. Suematsu, "Density-matrix theory of semiconductor lasers with relaxation broadening model—Gain and gain-suppression in semiconductor lasers, *IEEE J. Quantum Electron.*, vol. QE-21, pp. 434–442, May 1985.
[15] K. Petermann, "Calculated spontaneous emission factor for double-heterostructure injection lasers with gain-induced waveguiding," *IEEE J. Quantum Electron.*, vol. QE-15, pp. 566–570, July 1979.
[16] R. Olshansky, P. Hill, V. Lanzisera, and W. Powazinik, "Frequency response of 1.3 μm InGaAsP high speed semiconductor lasers," *IEEE J. Quantum Electron.*, vol. QE-23, pp. 1410–1418, Sept. 1987.
[17] T. Kimura and A. Sugimura, "Coupled phase-shift distributed-feedback semiconductor lasers for narow linewidth operation," *IEEE J. Quantum Electron.*, vol. QE-25, pp. 678–683, Apr. 1989.

Geert Morthier, for a photograph and biography, see p. 1723 of the June 1991 issue of this JOURNAL.

Frank Libbrecht was born in Kortrijk, Belgium, on September 22, 1964. He received the degree in electrical engineering and the Ph.D. degree from the University of Gent in 1987 and 1991, respectively. During his graduate work he was supported by the IWONL, the Belgian Institute for Scientific Research in Industry and Agriculture.

His main interests are in the field of modeling optical communication systems.

Klaus David, for a photograph and biography, see p. 1723 of the June 1991 issue of this JOURNAL.

Patrick Vankwikelberge, for a photograph and biography, see p. 1723 of the June 1991 issue of this JOURNAL.

Roel G. Baets (M'88), for a photograph and biography, see p. 787 of the March 1991 issue of this JOURNAL.